LETTER

doi:10.1038/nature21399

Decline in global oceanic oxygen content during the past five decades

Sunke Schmidtko[1], Lothar Stramma[1] & Martin Visbeck[1,2]

Ocean models predict a decline in the dissolved oxygen inventory of the global ocean of one to seven per cent by the year 2100, caused by a combination of a warming-induced decline in oxygen solubility and reduced ventilation of the deep ocean[1,2]. It is thought that such a decline in the oceanic oxygen content could affect ocean nutrient cycles and the marine habitat, with potentially detrimental consequences for fisheries and coastal economies[3–6]. Regional observational data indicate a continuous decrease in oceanic dissolved oxygen concentrations in most regions of the global ocean[1,7–10], with an increase reported in a few limited areas, varying by study[1,10]. Prior work attempting to resolve variations in dissolved oxygen concentrations at the global scale reported a global oxygen loss of 550 ± 130 teramoles (10^{12} mol) per decade between 100 and 1,000 metres depth based on a comparison of data from the 1970s and 1990s[10]. Here we provide a quantitative assessment of the entire ocean oxygen inventory by analysing dissolved oxygen and supporting data for the complete oceanic water column over the past 50 years. We find that the global oceanic oxygen content of 227.4 ± 1.1 petamoles (10^{15} mol) has decreased by more than two per cent (4.8 ± 2.1 petamoles) since 1960, with large variations in oxygen loss in different ocean basins and at different depths. We suggest that changes in the upper water column are mostly due to a warming-induced decrease in solubility and biological consumption. Changes in the deeper ocean may have their origin in basin-scale multi-decadal variability, oceanic overturning slow-down and a potential increase in biological consumption[11,12].

Dissolved oxygen observations of sufficient accuracy are available in the oceans since 1903 and the first basin-wide surveys were done in the 1920s (see Methods). Observations show ongoing regional changes in oceanic oxygen[1,7–10], and provide partial confirmation of climate models that predict an overall decline in oceanic oxygen concentrations, or 'deoxygenation', and a subsequent expansion of the mid-depth oxygen-minimum zones (OMZs) under global warming conditions[1,12,13]. Declining oxygen concentrations have also been found in coastal oceans, leading to more abundant and growing 'dead zones', regions of very low concentrations. Coastal changes have mostly been fuelled by riverine runoff of fertilizers[3], but in some cases may have been affected by the larger-scale oxygen changes. Dissolved oxygen loss has potentially broad impacts on pelagic and benthic fisheries, tourism, ocean nutrient cycling, and the oceanic source of N_2O, a potent greenhouse gas[3–6].

Oxygen decline in ocean models is linked to warming-induced declines in oxygen solubility, and reduced ventilation of deeper waters from enhanced upper-ocean stratification[1,2]. Changes detected over the past few decades have been attributed in part to these factors, but with additional complexities[10,14]. Regional long-term oxygen trends, as observed from time series stations for example[15], are superimposed with variations at interannual to multi-decadal timescales consistent with natural climate variability, including thermal and wind forcing changes from the North Atlantic Oscillation (NAO) in the Atlantic Ocean[16], the Southern Annular Mode (SAM) in the Southern Ocean, or the El Niño/Southern Oscillation (ENSO) and the Pacific Decadal Oscillation (PDO)[14]. In the low-latitude upper ocean, oxygen decline is attributed to a shoaling of the tropical and subtropical thermocline depth[14]. For other regions, explanations include warming-induced changes in solubility, wind forcing and large-scale ocean circulation[17].

Building on a limited analysis[10], we analyse the complete water column continuously since 1960, while working with a more extensive database (Extended Data Table 2; Extended Data Fig. 5) in combination with using rigorously tested data mapping[18,19] (see Methods). This enables a global fine-resolution linear trend analysis. The enlarged database allows quantitative assessment of the whole ocean oxygen inventory and its trend since 1960, more than quadrupling the volume previously analysed.

The global oceanic dissolved oxygen amounts to 227.4 ± 1.1 Pmol (Table 1); it is non-uniformly distributed (Fig. 1a) and reflects oceanic volume, bathymetry and deep-water ventilation rates. Large quantities of oxygen are found in the ventilated mixed-layer and a second maximum is found at greater depths (2,000–4,000 m) due to deep-water ventilation (Fig. 2a and c), with the latitudinal integrals mirroring the relative ocean volume distribution.

Many oceanic regions exhibit a loss of oxygen (Fig. 1b, Table 1) surpassing 4% per decade in isolated areas near OMZs (Extended Data Fig. 1). The largest decrease, 373 ± 165 Tmol, is found in the tropical and North Pacific Ocean. Both areas already have low oxygen concentrations below the thermocline. The largest absolute losses of oxygen, up to 30 mol m^{-2} per decade, are found in the Equatorial and North Pacific Ocean, the Southern Ocean and the South Atlantic Ocean.

The global oxygen loss of 961 ± 429 Tmol per decade since 1960 (Table 1) amounts to the loss of more than 4.8 ± 2.1 Pmol oxygen, which equals more than 2% of the total ocean inventory. Horizontally integrated oxygen change (Fig. 2d) indicates decreasing oxygen content throughout the water column, with a minimum rate of change at depths around 500 m. For the upper ocean, the large seasonal and interannual variability renders those trends barely significant[20], (Fig. 2d and Extended Data Table 1). The largest absolute and relative losses are observed in the main thermocline at 100–300 m depth as well as in mid-depth water masses (1,000–2,000 m). A large loss of oxygen is also observed from 2,000 m depth to the bottom. We analyse the possibility of a systematic bias and find that the existence of such a bias is unlikely and has a different distribution and smaller impact than the observed trends (see Methods, Extended Data Fig. 8).

The mixed layer oxygen is close to 100% saturation for the vast majority of the ocean. Variations in saturation are typically small and vary locally, with the exception of under-ice conditions in the polar regions. Below the thermocline, advection of surface waters and vertical mixing of saturated mixed layer waters are the only source of oxygen. Reduced ventilation and warming-induced solubility changes during the process of water mass formation can both lower the oxygen content of subsurface water masses[15]. Here we have to distinguish between reduced ventilation due either to a reduction in deep convection or to a reduction in mixed layer subduction. This will affect the mean

[1]GEOMAR Helmholtz Centre for Ocean Research Kiel, Düsternbrooker Weg 20, 24105 Kiel, Germany. [2]Kiel University, 24098 Kiel, Germany.

Table 1 | Oxygen content and change per basin

Basin	Oxygen content (Pmol)	Oxygen change (Tmol per decade)	Change as percentage of global change	Volume as percentage of global ocean volume
Arctic Ocean	4.7±0.2	−73±30	7.6±3.1	1.2
North Atlantic	26.9±0.1	−9±19	0.9±1.9	8.5
Equatorial Atlantic	15.9±0.0	−72±20	7.5±2.1	5.7
South Atlantic	22.4±0.1	−119±27	12.4±2.8	7.8
North Pacific	24.5±0.1	−173±40	18.0±4.2	16.3
Equatorial Pacific	25.5±0.4	−210±125	21.9±13.0	16.3
South Pacific	33.1±0.1	−71±37	7.4±3.9	14.3
Equatorial Indian Ocean	10.7±0.1	−55±49	5.7±5.1	6.6
South Indian Ocean	26.1±0.1	−27±34	2.8±3.5	10.2
Southern Ocean	37.6±0.1	−152±47	15.8±4.9	13.1
Total	**227.4±1.1**	**−961±429**	**100**	**100**

Trends that are more significant than two standard errors are marked in light grey. See Extended Data Table 1 for an extended version of this table.

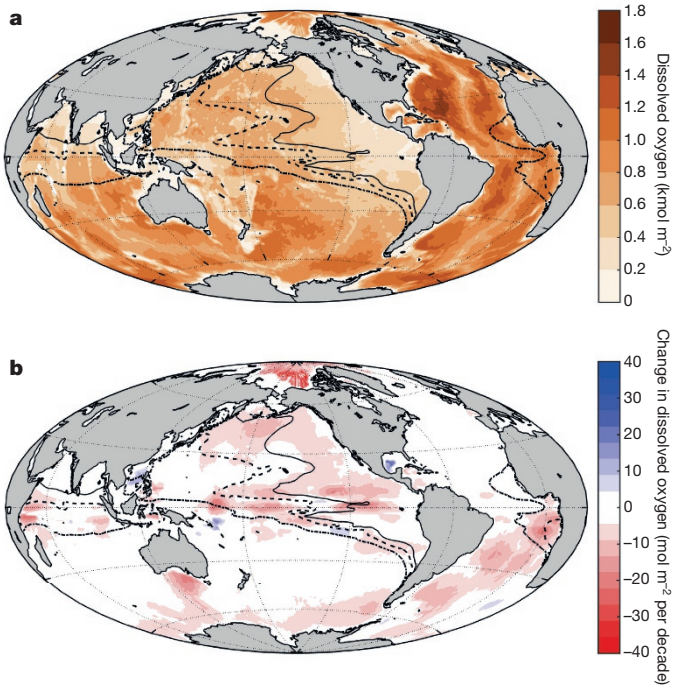

Figure 1 | Amount of dissolved oxygen and changes per decade since 1960. a, Global oxygen inventory (dissolved oxygen, colour coded). Lines indicate boundaries of oxygen-minimum zones (OMZs): dashed-dotted, regions with less than 80 μmol kg^{-1} oxygen anywhere within the water column; dashed lines and solid lines similarly represent regions with less than 40 μmol kg^{-1} oxygen and 20 μmol kg^{-1} oxygen, respectively. **b**, Change in dissolved oxygen per decade (colour coded). Lines show OMZs as in **a**.

oxygen distribution predominantly in newly formed water masses and propagate slowly through the oceans, while a meridional overturning circulation slowdown will affect the mean state globally, predominantly in regions with large oxygen gradients (see Methods).

Analysis of apparent oxygen utilization changes (Extended Data Fig. 1) indicates that thermally forced changes in solubility can account for about 130 Tmol of the observed oxygen loss (Fig. 2b, d and e, Extended Data Table 1, Methods). This solubility-related change strongly decreases with depth and is negligible below 1,000 m (Fig. 2d, Extended Data Fig. 2, Extended Data Table 1). Above 150 m, where oxygen is often supersaturated, the oxygen decrease is only half that expected from warming-induced solubility change, indicating a compensating trend towards greater supersaturation (Fig. 2e). Integrated over the top 1,000 m of the global oceans, about 50% of oxygen loss can be attributed to solubility changes (more at shallower levels); this value decreases to about 25% when integrated over the top 2,000 m (Fig. 2e). This deep-reaching impact of thermally driven oxygen changes in the integrative figures is due to the strong solubility effect in the near surface ocean, partly supporting earlier results[10].

A full depth analysis reveals that of the order of 15% (0.7 Pmol) of the overall observed oxygen loss since 1960 can be attributed to oceanic warming induced solubility changes (Fig. 2e, Extended Data Figs 2 and 3, Extended Data Table 1). Observed changes in salinity (Extended Data Fig. 3) are too small to have significant impact on oxygen solubility. Consumption changes are unlikely to be large below 1,000 m (ref. 21), because the main cause of oxygen consumption, remineralization, is assumed to be strongly decreasing with depth[1], though the indicated increased supersaturation in shallow waters weakens this assumption. Consumption changes at depth due to increased surface biological activity would have an enhanced impact in the upper water column, decreasing with depth. This suggests that either multi-decadal variations or changes in ocean circulation induced ventilation, potentially enhanced by increased upper ocean biological activity, are responsible for the observed changes in oxygen below 1,000 m.

Waters below the thermocline, at intermediate depths of 400–700 m, show minimal oxygen decline (Fig. 2d; Extended Data Fig. 4). The oxygen loss observed at these depths is similar to the loss expected from thermally forced solubility changes (Fig. 2d). Whereas deep waters are largely formed by thermal buoyancy loss from interplay with strong winds at higher latitudes, a large fraction of the intermediate waters are formed by subduction due to wind stress forcing[22].

Five distinct regions with significant oxygen loss stand out that cannot be attributed to solubility changes. These are (1) tropical regions of all basins, which contain most of the upper ocean OMZ, (2) the North Pacific, (3) the South Atlantic, (4) the Southern Ocean and (5) the Arctic Ocean (Table 1, Fig. 1b, Extended Data Fig. 4).

The changes in the North and Equatorial Pacific account for the largest fraction of global oxygen loss, 39.9 ± 17.2%, and are collocated with low amounts of oxygen below the thermocline. Thus impacts on the ecosystem[23] and on possible future climate change[24] are likely here. The volume of waters with anoxic conditions has more than quadrupled over the time period analysed, with a number of biochemical consequences, including enhanced marine production of N_2O (ref. 25). North Pacific oxygen decrease shows little to no decadal variability below 1,000 m (Fig. 3a), indicating that PDO variations are unlikely to play a role in the basin-wide oxygen inventory and the long term decline in the deep North Pacific. In the upper water column, changes on the timescale of the PDO are observed (Fig. 3a). Here formation of North Pacific Intermediate Water (NPIW) is thought to be the main source of oxygen, for example[26]. Long term surface warming in the formation region probably contributed to declining intermediate water formation rates[27].

Oxygen losses in the Southern Ocean (15.8 ± 4.9% of the global loss) are the second largest fraction of the global oxygen loss. They are consistent with the observed decline of deep water formation of Antarctic water masses[28] and may also represent changes in the wind field, because Southern Ocean ventilation is tied to both thermal buoyancy and changes in circumpolar wind patterns. Oxygen changes are most pronounced in the Indian and Pacific sectors of the Southern Ocean, mirroring the observed long term increase in Antarctic Bottom Water (AABW) salinity and in the temperature of the circumpolar deep water[19], both most pronounced in the Indian and Pacific sector.

12.4 ± 2.8% of the global oxygen loss is found in the South Atlantic Ocean (Table 1) and is spread over the entire deep-water column

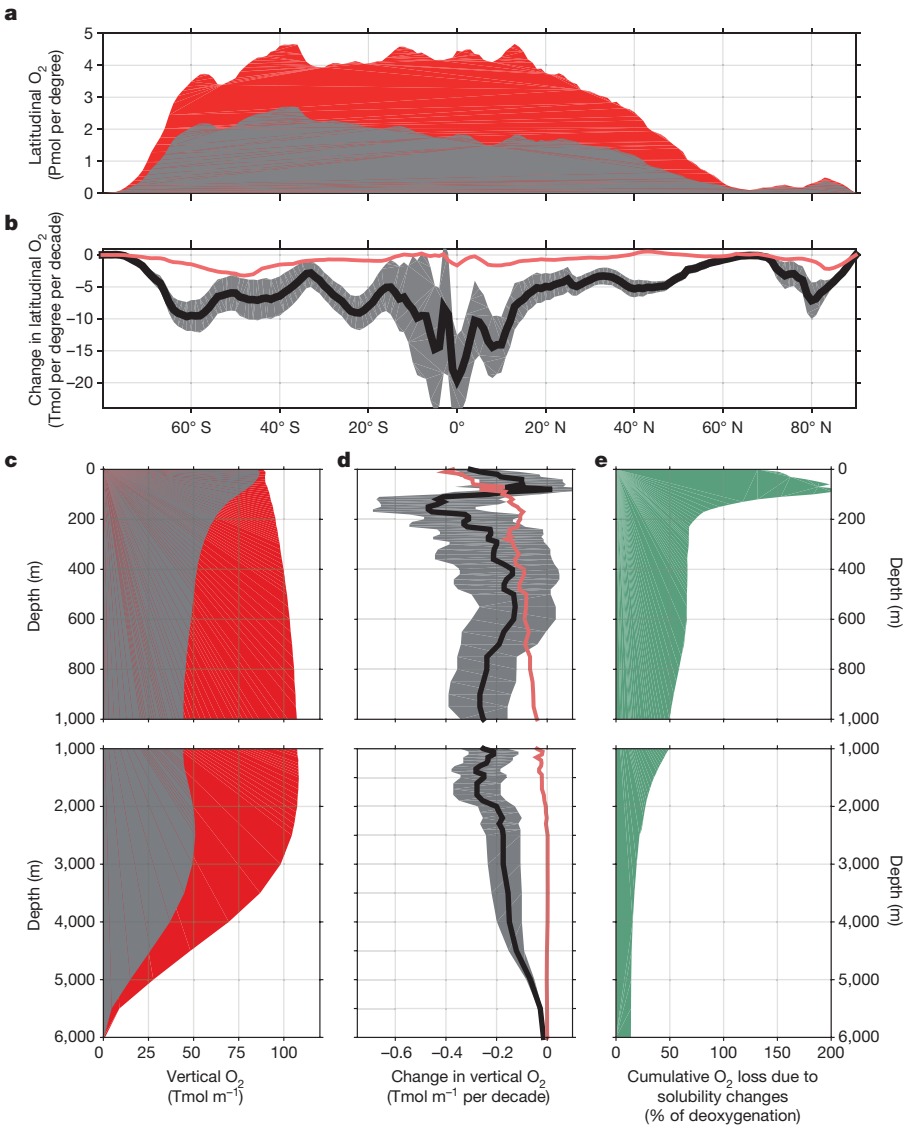

Figure 2 | Oxygen content and change per decade over the past five decades. a–d, Latitudinal dissolved oxygen (**a**) and its change per decade (**b**); vertical dissolved oxygen (**c**) and its change per decade (**d**). In **a** and **c**, integrated dissolved oxygen is shown as the grey area, and apparent oxygen utilization as the red area; together they show the maximum possible amount of oxygen, that is, 100% saturation. In **b** and **d**, oxygen change is indicated as the black line with the error as the grey envelope, the red line indicates the loss expected from solubility changes alone. **e**, Water column cumulative oxygen loss due to solubility change as a percentage of observed deoxygenation. Solubility changes above 100% are due to processes that increase the upper ocean oxygen content and counteract the warming.

between North Atlantic Deep Water and Antarctic Bottom Water (Extended Data Fig. 4, Extended Data Table 1). The oxygen change is in line with reduced ventilation due to meridional overturning changes; this reduced ventilation has provided less oxygenated waters in recent years (Fig. 3g, Extended Data Fig. 4). However, here the observed oxygen changes are too large to be entirely explained by a declining overturning alone, as they would require a complete overturning shut down (see Methods). Since similar oxygen decrease is not apparent in the North Atlantic, the oceanic dynamics at play are restricted to the South Atlantic (Fig. 1b, Table 1). A time series analysis in the South Atlantic (Fig. 3g) indicates that this trend does not hold true for earlier decades and thus is most likely to be related to multi-decadal variability, but the origin of this variability cannot be explained yet. Since this variability is limited to the South Atlantic basin, regional changes in biological activity and South Atlantic overturning pathways, such as the separation of the deep western boundary current, are likely to play a role.

We also find that the Arctic Ocean has lost 73 ± 30 Tmol of oxygen, despite a small Arctic Ocean oxygen inventory (4.7 ± 0.2 Pmol). This loss contributes $7.6 \pm 3.1\%$ of the global oxygen loss while the Arctic contains less than 1.2% of the global oceanic volume. Only the Russian shelf shows increasing oxygen levels, probably related to decreasing winter sea-ice coverage[29]. Since solubility-related oxygen changes are less than one-third in Arctic low temperature environments, the most likely cause of the declining dissolved oxygen is reduced deep water ventilation due to a freshening and warming in the Canada Basin and the Beaufort Sea[30] (Extended Data Figs 3 and 4), though the reduction of summer sea ice in the area might have increased biological activity to the extent that parts of the oxygen loss have to be attributed to consumption changes.

Oxygen data in the Arctic, Equatorial and North Pacific (below 1,000 m) and Southern Ocean show a continuous decrease, and together are responsible for more than 60% of the global oceanic oxygen loss. This could either be due to multi-decadal variability, as proposed for the South Atlantic, or to a circulation-induced reduced ventilation, probably caused by a reduced thermal buoyancy loss and changes in the wind fields at higher latitudes, for example[31]. However, in the upper 1,000 m of the global ocean, solubility changes are the dominant factor for deoxygenation (Fig. 2e). The amount of oxygen loss related to deep

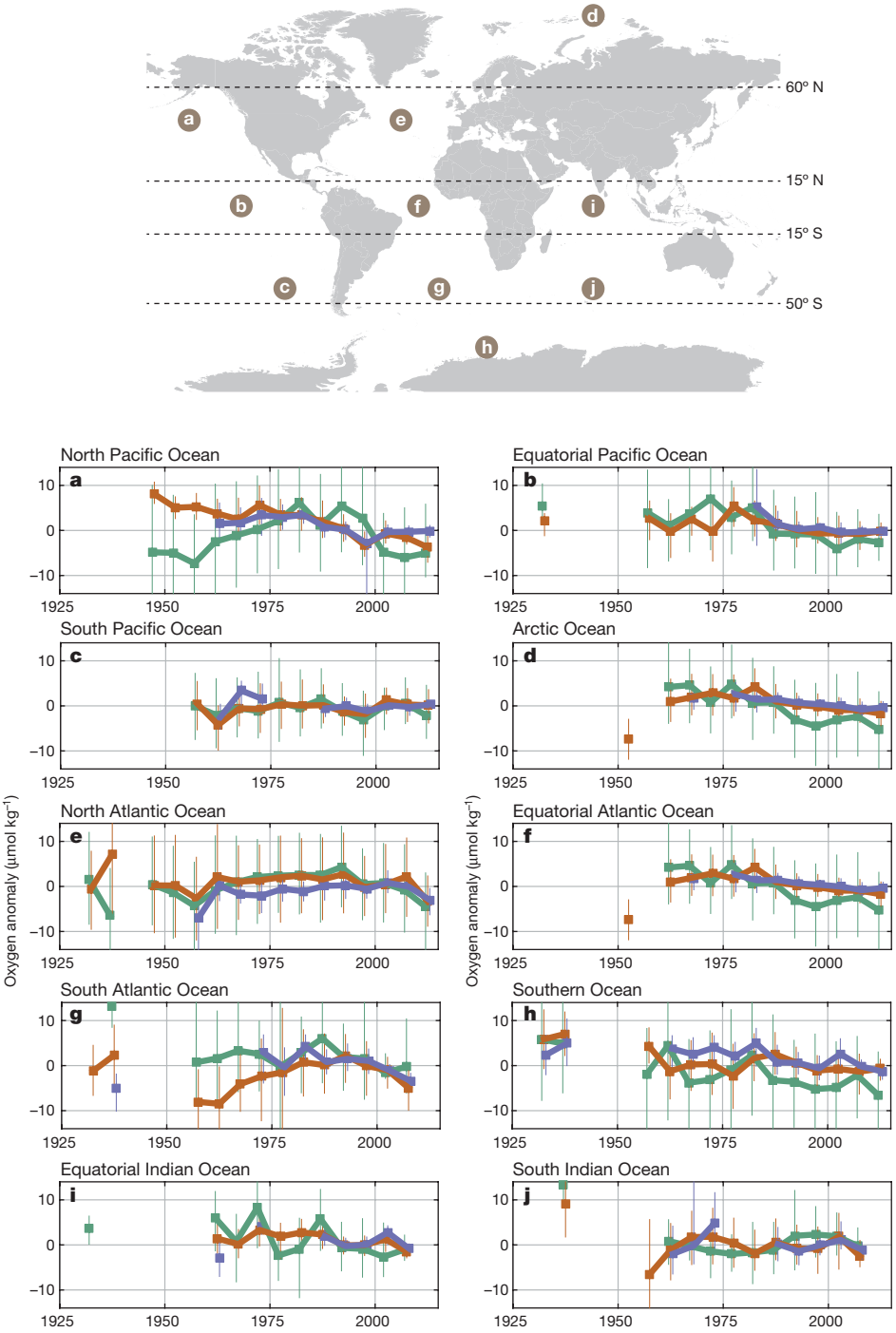

Figure 3 | Oxygen time series for ocean basins. a–j, Plots of semi-decadal median oxygen anomalies in μmol kg^{-1} (vertical axis; squares) with interquartile ranges (whiskers) at depths in the basins of 300 m (green), 1,000 m (orange) and 3,000 m (blue). Temporal intervals with more than 20 observations are shown. Map at top shows approximate positions of the ocean basins; plots **a–j** are labelled with the name of the basin at the top. Area boundaries (dashed lines) are 60° N, 15° N, 15° S and 50° S.

ocean decadal variability cannot be quantified yet, but is a part of the described losses. Consumption changes might contribute to this loss[12], but are unlikely to be the major source of oxygen loss. Since oxygen is a good integrative water age tracer in the deep ocean, oxygen changes provide global scale observational evidence for changes in deep ocean water mass distribution[11,28].

Our oxygen budget reveals that thermally driven deep and intermediate waters have been losing 703 ± 244 Tmol of oxygen per decade. A global quantification between multi-decadal variability and a reduced overturning remains elusive, and requires more time series data and local analyses. Similarly, the onset of this linear decrease cannot be identified with this data set on the global scale. Oxygen decrease patterns expected from anthropogenic warming[2] have large similarities with the distribution detected here. The implications of this ocean oxygen inventory change for the oceanic part of the global carbon budget are discussed in the Methods.

The oxygen inventory predicted by climate models varies[32], but spans today's observed levels. The observed global oxygen decline of nearly 1 Pmol per decade exceeds model estimates, which range from 0 to 600 Tmol per decade[32], but the observed inventory changes

mirror expected patterns from anthropogenic warming[2]. Some of the model-based scenarios are consistent with observed oxygen declines in individual basins[2,20]. The observed warming-induced change, 15% of the overall oxygen decline, is currently less than predicted by models for the next century[13], indicating that the models currently underestimate the potential for non-solubility related O_2 changes. Models predict an accelerating oxygen loss of up to 125 Tmol yr^{-1} by 2100[13], which is 25% more than the currently observed decline, emphasizing the longer term cumulative impacts of ocean dynamics on dissolved oxygen. Such an oxygen loss sums up to more than 8 Pmol by 2100, consistent with the assumption of an increasing volume of anoxic waters; this loss is expected to result in substantial changes in ocean ecosystems and in ocean–climate feedback through production of N_2O. Far-reaching implications for marine ecosystems and fisheries can be expected[23].

Online Content Methods, along with any additional Extended Data display items and Source Data, are available in the online version of the paper; references unique to these sections appear only in the online paper.

Received 24 November 2015; accepted 18 January 2017.

1. Keeling, R. F., Körtzinger, A. & Gruber, N. Ocean deoxygenation in a warming world. *Annu. Rev. Mar. Sci.* **2,** 199–229 (2010).
2. Long, M. C., Deutsch, C. A. & Ito, T. Finding forced trends in oceanic oxygen. *Glob. Biogeochem. Cycles* **30,** 381–397 (2016).
3. Diaz, R. J. & Rosenberg, R. Spreading dead zones and consequences for marine ecosystems. *Science* **321,** 926–929 (2008).
4. Stramma, L. *et al.* Expansion of oxygen minimum zones may reduce available habitat for tropical pelagic fishes. *Nat. Clim. Change* **2,** 33–37 (2011).
5. Vaquer-Sunyer, R. & Duarte, C. M. Thresholds of hypoxia for marine biodiversity. *Proc. Natl Acad. Sci. USA* **105,** 15452–15457 (2008).
6. Worm, B. Global patterns of predator diversity in the open oceans. *Science* **309,** 1365–1369 (2005).
7. Stramma, L., Johnson, G. C., Sprintall, J. & Mohrholz, V. Expanding oxygen-minimum zones in the tropical oceans. *Science* **320,** 655–658 (2008).
8. Whitney, F. A., Freeland, H. J. & Robert, M. Persistently declining oxygen levels in the interior waters of the eastern subarctic Pacific. *Prog. Oceanogr.* **75,** 179–199 (2007).
9. Bograd, S. J. *et al.* Oxygen declines and the shoaling of the hypoxic boundary in the California Current. *Geophys. Res. Lett.* **35,** L12607 (2008).
10. Helm, K. P., Bindoff, N. L. & Church, J. A. Observed decreases in oxygen content of the global ocean. *Geophys. Res. Lett.* **38,** L23602 (2011).
11. Broecker, W. S., Sutherland, S. & Peng, T.-H. A possible 20th-century slowdown of Southern Ocean Deep Water formation. *Science* **286,** 1132–1135 (1999).
12. Keller, D. P., Kriest, I., Koeve, W. & Oschlies, A. Southern Ocean biological impacts on global ocean oxygen. *Geophys. Res. Lett.* **43,** 6469–6477 (2016).
13. Bopp, L., Le Quéré, C., Heimann, M., Manning, A. C. & Monfray, P. Climate-induced oceanic oxygen fluxes: implications for the contemporary carbon budget. *Glob. Biogeochem. Cycles* **16,** http://dx.doi.org/10.1029/2001GB001445 (2002).
14. Deutsch, C., Brix, H., Ito, T., Frenzel, H. & Thompson, L. Climate-forced variability of ocean hypoxia. *Science* **333,** 336–339 (2011).
15. Keeling, R. F. & García, H. E. The change in oceanic O_2 inventory associated with recent global warming. *Proc. Natl Acad. Sci. USA* **99,** 7848–7853 (2002).
16. Stendardo, I. & Gruber, N. Oxygen trends over five decades in the North Atlantic. *J. Geophys. Res.* **117,** C11004 (2012).
17. Deutsch, C. A., Emerson, S. & Thompson, L. Fingerprints of climate change in North Pacific oxygen. *Geophys. Res. Lett.* **32,** L16604, http://dx.doi.org/10.1029/2005GL023190 (2005).
18. Schmidtko, S., Johnson, G. C. & Lyman, J. M. MIMOC: A global monthly isopycnal upper-ocean climatology with mixed layers. *J. Geophys. Res. Oceans* **118,** 1658–1672 (2013).
19. Schmidtko, S., Heywood, K. J., Thompson, A. F. & Aoki, S. Multidecadal warming of Antarctic waters. *Science* **346,** 1227–1231 (2014).
20. Frölicher, T. L., Joos, F., Plattner, G. K., Steinacher, M. & Doney, S. C. Natural variability and anthropogenic trends in oceanic oxygen in a coupled carbon cycle-climate model ensemble. *Glob. Biogeochem. Cycles* **23,** GB1003, http://dx.doi.org/10.1029/2008GB003316 (2009).
21. Bianchi, D., Galbraith, E. D., Carozza, D. A., Mislan, K. A. S. & Stock, C. A. Intensification of open-ocean oxygen depletion by vertically migrating animals. *Nat. Geosci.* **6,** 545–548 (2013).
22. Wyrtki, K. The thermohaline circulation in relation to the general circulation in the oceans. *Deep-Sea Res.* **8,** 39–64 (1961).
23. Cheung, W. W. L. *et al.* Shrinking of fishes exacerbates impacts of global ocean changes on marine ecosystems. *Nat. Clim. Change* **3,** 254–258 (2012).
24. Codispoti, L. A. Interesting times for marine N_2O. *Science* **327,** 1339–1340 (2010).
25. Santoro, A. E., Buchwald, C., McIlvin, M. R. & Casciotti, K. L. Isotopic signature of N_2O produced by marine ammonia-oxidizing Archaea. *Science* **333,** 1282–1285 (2011).
26. Kwon, E. Y., Deutsch, C. A., Xie, S.-P., Schmidtko, S. & Cho, Y.-K. The North Pacific Oxygen uptake rates over the past half century. *J. Clim.* **29,** 61–76 (2016).
27. Watanabe, Y. W. *et al.* Probability of a reduction in the formation rate of the subsurface water in the North Pacific during the 1980s and 1990s. *Geophys. Res. Lett.* **28,** 3289–3292 (2001).
28. Purkey, S. G. & Johnson, G. C. Global contraction of Antarctic bottom water between the 1980s and 2000s. *J. Clim.* **25,** 5830–5844 (2012).
29. Kwok, R. & Rothrock, D. A. Decline in Arctic sea ice thickness from submarine and ICESat records: 1958–2008. *Geophys. Res. Lett.* **36,** L15501, http://dx.doi.org/10.1029/2009GL039035 (2009).
30. Morison, J. *et al.* Changing Arctic Ocean freshwater pathways. *Nature* **481,** 66–70 (2012).
31. Biastoch, A., Böning, C. W., Getzlaff, J., Molines, J.-M. & Madec, G. Causes of interannual–decadal variability in the meridional overturning circulation of the midlatitude North Atlantic Ocean. *J. Clim.* **21,** 6599–6615 (2008).
32. Cocco, V. *et al.* Oxygen and indicators of stress for marine life in multi-model global warming projections. *Biogeosciences* **10,** 1849–1868 (2013).

Acknowledgements S.S. was supported by the German Federal Ministry of Education and Research project MIKLIP, and L.S. and M.V. by the German Research Foundation (DFG) as part of research project SFB-754. We thank R. Keeling for providing expertise on chemical processes of oxygen measurements and calculating impacts on carbon budgeting.

Author Contributions S.S. designed the experiment and did the computations and data analysis; L.S. and S.S. evaluated the analysis; and M.V. provided expertise on ocean ventilation and computations. All authors discussed the results and wrote the manuscript.

Author Information Reprints and permissions information is available at www.nature.com/reprints. The authors declare no competing financial interests. Readers are welcome to comment on the online version of the paper. Correspondence and requests for materials should be addressed to S.S. (sschmidtko@geomar.de).

Reviewer Information *Nature* thanks S. Doney, D. Gilbert and the other anonymous reviewer(s) for their contribution to the peer review of this work.

METHODS

Data handling. We combined salinity, temperature, depth, oxygen (CTD and bottles) profiles from five publicly available databases (Extended Data Table 2) and mapped the properties on 78 depth levels of the global ocean since 1960. We assume the error in the data over the decades to be noise rather than systematic, since oxygen calibration, done with the Winkler titration method, has changed little over time, and several method comparison studies and long term trend analysis did not reveal a significant long term bias[33–35]. CTD data are assumed to be calibrated by Winkler method, comparing bottle and CTD data revealed no bias between these data sources. Still, from the current state of knowledge about Winkler method the existence of a systematic bias cannot be fully ruled out. The impact of a possible systematic bias[33–35] is tested with a sensitivity analysis and is presented below. A similar procedure is performed on the assumption of overestimation of historic measurements in very low oxygen environments. Only data points with all four variables within physically plausible limits were used. Anomalies were computed since 1925 for each profile referenced to the mapped properties. Owing to limited data (Extended Data Fig. 5) in remote areas, not all regions resolve the same period (Extended Data Fig. 6). Duplicates were avoided by checking for repeat profiles within 5 km and 25 h, allowing for rounding errors in latitude, longitude and time. In the rare case that two or more oxygen casts were made within these temporal and spatial scales, we treat them as duplicates and only use one. When duplicate profiles were identified, the profile with the best vertical resolution was used. Next to the database quality control flags, several filters were applied. Profiles with a difference of less than 5 μmol kg^{-1} between maximum and minimum observed oxygen were removed, as well as profiles with oxygen difference of less than 0.5 μmol kg^{-1} within 18 depth levels; these methods do exclude profiles with constant values as well as profiles which were stored with the wrong unit description (commonly ml l^{-1}). Furthermore, profiles with less than 100 μmol kg^{-1} oxygen at the surface were removed. Additional quality control measures were the removal of profiles with supersaturation at depths deeper than 200 m as well as supersaturation above 115%.

After quality control and duplicate removal, to avoid an increase in bias by clusters of data, all profiles within 0.25° (in latitude and longitude) and 3 months are median-binned.

We apply the ETOPO-1 bathymetry for our analysis[36]. For each grid point in our maps, the horizontal distance to data positions is derived by a fast marching algorithm[18,19]. The algorithm uses logarithmic scaling in bathymetry difference and a minimum propagation of 0.05 on a 18×18 km grid spacing for the speed map[18]. This algorithm determines the along-path distance between the grid point to be mapped and data locations, including distance penalties for moving across bathymetry with different depths. Over the continental slope, the mapping is predominantly along bathymetric contours. Over flat bathymetry, the algorithm would result in a circular region of influence, however over rough, highly variable terrain, the distances may be significantly longer in some directions (see supplementary information of ref. 19). Only data at locations that can be reached with this marching algorithm are used. Grid points are only mapped if more than 20 data points within 2,000 km virtual distance are found. This relates to a real world physical distance of 100 km to 2,000 km depending on location. Data are normally weighted using an along-pathway horizontal scaling of 1,000 km. To reduce the bias of El Niño and La Niña conditions in the equatorial regions, an Oceanic Niño Index (ONI)[37] normally weighted with a scaling of 0.4 for equatorial data with Gaussian decay towards higher latitude using a 10° scaling is applied.

As a final step before mapping, an interquartile range (IQR) filter is applied to all parameters. Values more than one IQR below the first quartile or more than one IQR above the third quartile are rejected: this is equivalent to using 95% of the data for a normal distribution. We then apply a weighted least-squares model[38] (LOESS) at each grid point to all data with positive weights larger than 10^{-6}. The model removes linear and quadratic fits for longitude and latitude in the fast marching-derived coordinate system[4,18,19].

This LOESS model is used to determine the mean state and temporal trend of water mass properties in temperature, salinity and oxygen. The spatial trend removal in the fast marching-derived coordinate system accounts for across and along slope gradients for any resolved bathymetry[18]. The model is restrained to the range of observed values that passed IQR filtering for the mean state. Mapped values with errors for the mean larger than 100 μmol kg^{-1} and errors in trend larger than 35 μmol kg^{-1} were removed; these were found in isolated canyons of mid-ocean ridges and below the sea-ice close to Antarctica in the Indian Ocean sector.

We regard trends as significant that are larger than twice the 'estimated standard error' of the least squares solution. To derive oxygen changes due to solubility, trends in apparent oxygen utilization (AOU) and dissolved oxygen are subtracted.

The 5-yr median properties for the different regions (Fig. 3) are computed from the anomalies in respect to the climatological mean as computed above. Median anomalies and IQR from all profiles within defined regions were computed. No spatial adjustments were made and no trends computed from these 5-yr median bins.

Ventilation, overturning and consumption. From our current understanding of the oceans, the oxygen loss in the deep oceans can have four origins. (a) A reduction of ventilation in deep convection regions, which would provide less ventilated waters in high latitudes, and a reduction of mixed layer subduction, mainly in mid and high latitudes. (b) A slowdown of meridional overturning circulation, which would reduce the amount of oxygenated waters that are mixed with older waters and thus increase the age of the deep waters in general. (c) An increase in biological activity in the upper ocean, with increased remineralization and thus oxygen consumption at depth. (d) Natural multi-decadal variability that is not captured by the data currently available.

While we cannot assign the observed changes to a sole origin, some are more likely than others. Reduced ventilation by deep convection is going to have a slow impact, since the oxygen-reduced waters will have to advect throughout the global basins before affecting older water masses. A reduction in deep convection that happens now might be observed in the tropical oceans in 50–100 years, assuming no impact on overturning transports by a reduced deep water convection. On the other hand, a reduction of meridional overturning circulation (MOC) will be observed globally instantaneously, since a reduction of MOC reduces the 'push' of oxygenated waters into areas deprived of oxygen. The last cause for accelerated oxygen decrease at depth is an increased remineralization, caused by enhanced biological activity. This would increase oxygen consumption throughout the water column, though decreasing with depth, since the Martin curve decreases close to exponentially.

Stability of oxygen measurements and the likelihood of systematic bias. The chemical analysis methods have essentially not changed, allowing for fairly robust estimation of long-term trends. To estimate the impact of a possible systematic bias[34] resulting from possible long-term variations in the purity of chemical reagents used in the Winkler method, we added an artificial bias to an identical duplicate data set, increasing 50 year old oxygen values by 0.5%, with the bias linearly decreasing to zero by the year 2000. This imitates the effect of impurities in the chemical reagents leading to larger quantities of solution used in the Winkler method, leading to a positive bias in historic oxygen measurements. The complete computation is performed and the original derived trends were then subtracted from the final computations. The remaining fields are presented in Extended Data Fig. 7 and only contain the pattern and distribution of the mapped systematic bias that was added to the data, the trends are an order of magnitude smaller than the observed trends of Extended Data Fig. 4. The oxygen loss of the artificial systematic bias would amount to 230 Tmol per decade, compared to the observed 960 Tmol per decade, though with the majority of oxygen loss differently distributed to that observed. Thus in the unlikely case that a bias of 0.5% is within the data, it could only explain 24% of the observed oxygen decrease. A bias of the order of 1% subsequently leads to an oxygen decrease on the order of 48% of the observed trend. Since the pattern and distribution of this artificial oxygen loss differ notably from the observed pattern, an attribution of this order is very unlikely. However, we note that a systematic bias leading to a decrease of the order of 10–15% of the observed trend would be under the detection threshold and cannot be completely ruled out.

Another possible bias of historical measurements is the overestimation of oxygen in very low oxygen environments by 2–4 μmol kg^{-1}. We test the impact of such a bias by excluding all negative trends in low oxygen waters (<15 μmol kg^{-1}) from the trend analysis. The resulting global oxygen loss would then amount to 935 Tmol per decade, 2.5% lower than the value presented in this Letter. Therefore we can assume that this bias, if present, has no impact on the main finding of this Letter.

Verification of mapping bias. To verify the mapping of oxygen trends, temperature and salinity data were handled identically to oxygen data, using the same subset of temperature and salinity data points. Since salinity and temperature trends have distinct, different patterns to oxygen, these results confirm that no large scale mapping induced trend is created (Extended Data Fig. 3). A reduction in data density to randomly selected 30,000 and 20,000 profiles per decade leads to nearly identical global trends with larger error, further indicating the robustness of the mapping method despite limited observations (Extended Data Fig. 8).

Changes in the South Atlantic. The western South Atlantic at 1,500 to 4,500 m has a mean oxygen content of the order of 200 μmol kg^{-1} in the range between 15° S and 35° S, and the oxygen content on the eastern side is about 20 μmol kg^{-1} lower. Assuming the South Atlantic Meridional Overturning Cell with 20 Sv passing eastwards through this window, this would provide about 126 Tmol of oxygen per decade. The observed change of 120 Tmol per decade in the South Atlantic is of the same order. Since a complete shutdown of the South Atlantic Overturning Cell is unlikely, a change in circulation or upstream changes probably do play a role.

Carbon budget impacts. The change we resolve in the ocean oxygen (O_2) inventory has implications for carbon accounting. The reduction in deep water

convection or MOC slow down, as implied by the O_2 data, must have reduced the oceanic uptake of anthropogenic CO_2 by slowing the mixing of excess carbon into the ocean interior. The reduction also must have increased the efficiency of the ocean biological carbon pump, which naturally sequesters carbon in the deep ocean. While these processes mechanistically will have partly counteracted each other, they will not have counteracted each other in terms of carbon accounting. Any slowing of ventilation that began 50 or more years ago must be already effectively included in estimates of the recent uptake of anthropogenic CO_2 based on measurements of transient tracers, such as CFC-11 (see, for example, ref. 39), because these approaches are based on constraints on ocean mixing over the past few decades. The slowing effect on the biological pump will have been neglected by these methods, however. Relating changes in O_2 inventory to carbon inventory is complex because of buffering effects on air–sea CO_2 exchange[40]. As a rough estimate, assuming a scaling of -2.5 mol O_2 per mol C (ref. 40), the ventilation-induced decrease in oxygen below 1,200 m suggests a ventilation-induced deep carbon inventory increase of $0.6\times10^{15}/2.5=0.24$ Tmol C per decade or 0.3 Pg C yr^{-1} with large uncertainties. The total ocean CO_2 uptake would then be 0.3 Pg C yr^{-1} higher than currently estimated based on the transient tracer approaches. In addition, the decrease in ocean oxygen inventory must be closely matched by a comparable release of oxygen to the atmosphere, with implications for CO_2 budgets based on changes in atmospheric oxygen[40]. For example, a recent oxygen based estimate of the ocean sink of 2.45 Pg C yr^{-1} over 1991–2011[41] would need revision to 2.83 Pg C yr^{-1}, associated with revising the oceanic oxygen release from 0.49×10^{15} to 0.84×10^{15} mol oxygen per decade.

Sample size. No statistical methods were used to predetermine sample size

Data availability. All data supporting the findings of this study are publically available as referenced within the paper and in Extended Data Table 2. The mapping script and fast marching script are available from the corresponding author on reasonable request.

33. Carpenter, J. H. The accuracy of the Winkler method for dissolved oxygen analysis. *Limnol. Oceanogr.* **10,** 135–140 (1965).
34. Wilcock, R. J., Stevenson, C. D. & Roberts, C. A. An interlaboratory study of dissolved oxygen in water. *Water Res.* **15,** 321–325 (1981).
35. Knapp, G. P., Stalcup, M. C. & Stanley, R. J. Iodine losses during Winkler titrations. *Deep-Sea Res. A* **38,** 121–128 (1991).
36. Amante, C. & Eakins, B. W. *ETOPO1 1 Arc-minute Global Relief Model: Procedures, Data Sources and Analysis.* NOAA Technical Memorandum NESDIS NGDC-24, http://dx.doi.org/10.7289/V5C8276M (NOAA, National Geophysical Data Center, 2009).
37. *Oceanic Niño Index* (ONI) (NOAA Climate Prediction Center); available at http://www.cpc.ncep.noaa.gov/products/analysis_monitoring/ensostuff/ensoyears.shtml (accessed 24 March 2014).
38. Cleveland, W. S. Robust locally weighted regression and smoothing scatterplots. *J. Am. Stat. Assoc.* **74,** 829–836 (1979).
39. Khatiwala, S., Primeau, F. & Hall, T. Reconstruction of the history of anthropogenic CO_2 concentrations in the ocean. *Nature* **462,** 346–349 (2009).
40. Keeling, R. F. & Severinghaus, J. P. in *The Carbon Cycle* (eds Wigley, T. M. L. & Schimel, D.) 134–140 (Global Change Institute, Proceedings on the Carbon Cycle, Cambridge Univ. Press, 2000).
41. Keeling, R. F. & Manning, A. C. in *Treatise on Geochemistry* 2nd edn (eds Turekian, K. & Holland, H.) 385–404 (Elsevier, 2014).

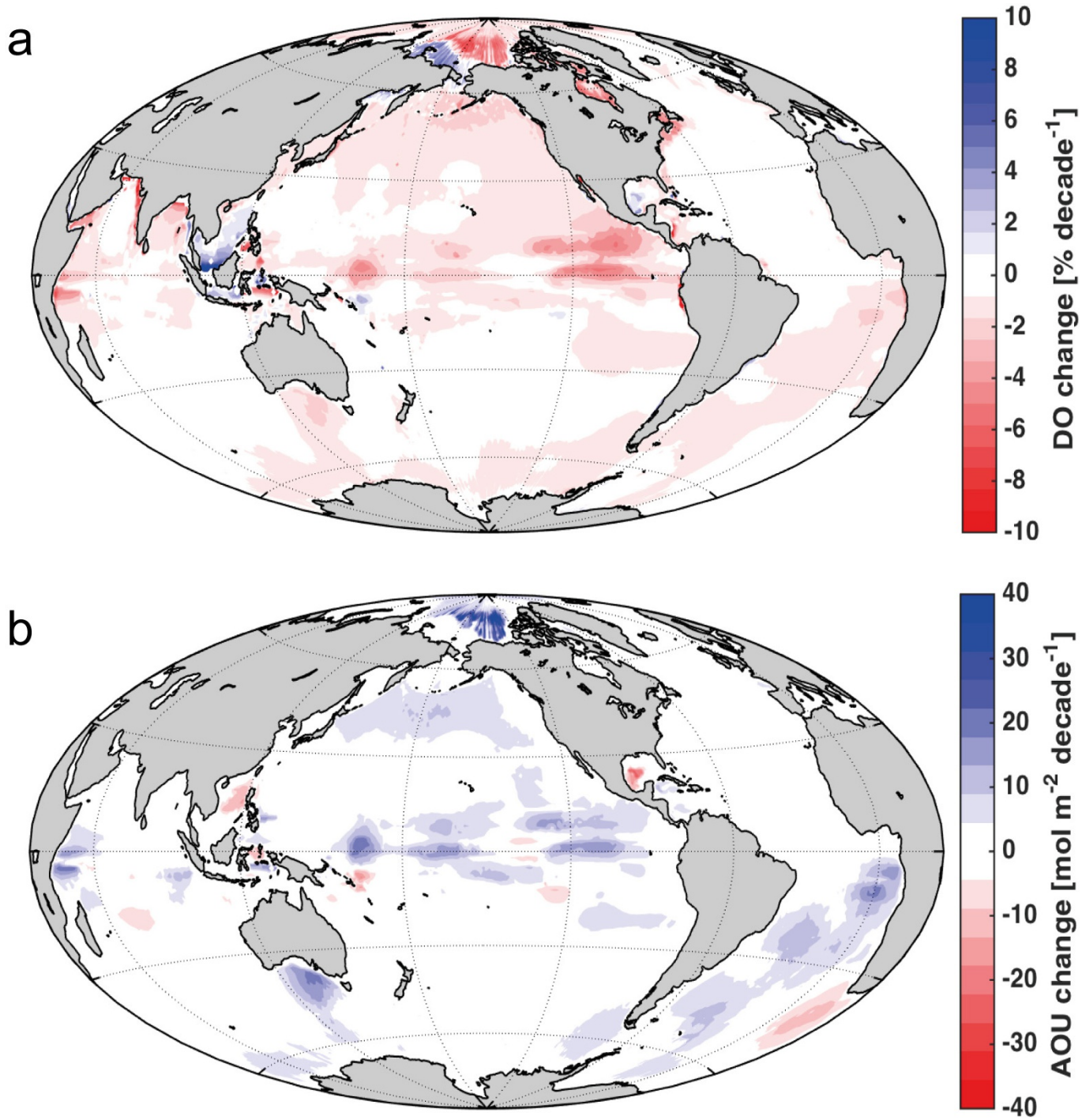

Extended Data Figure 1 | Dissolved oxygen and apparent oxygen utilization changes per decade since 1960. a, Change of dissolved oxygen (DO) per square metre per decade (in units of percentage of local dissolved oxygen); these data are similar to those in Fig. 1. **b**, Change of apparent oxygen utilization (AOU) in units of mol per square metre per decade.

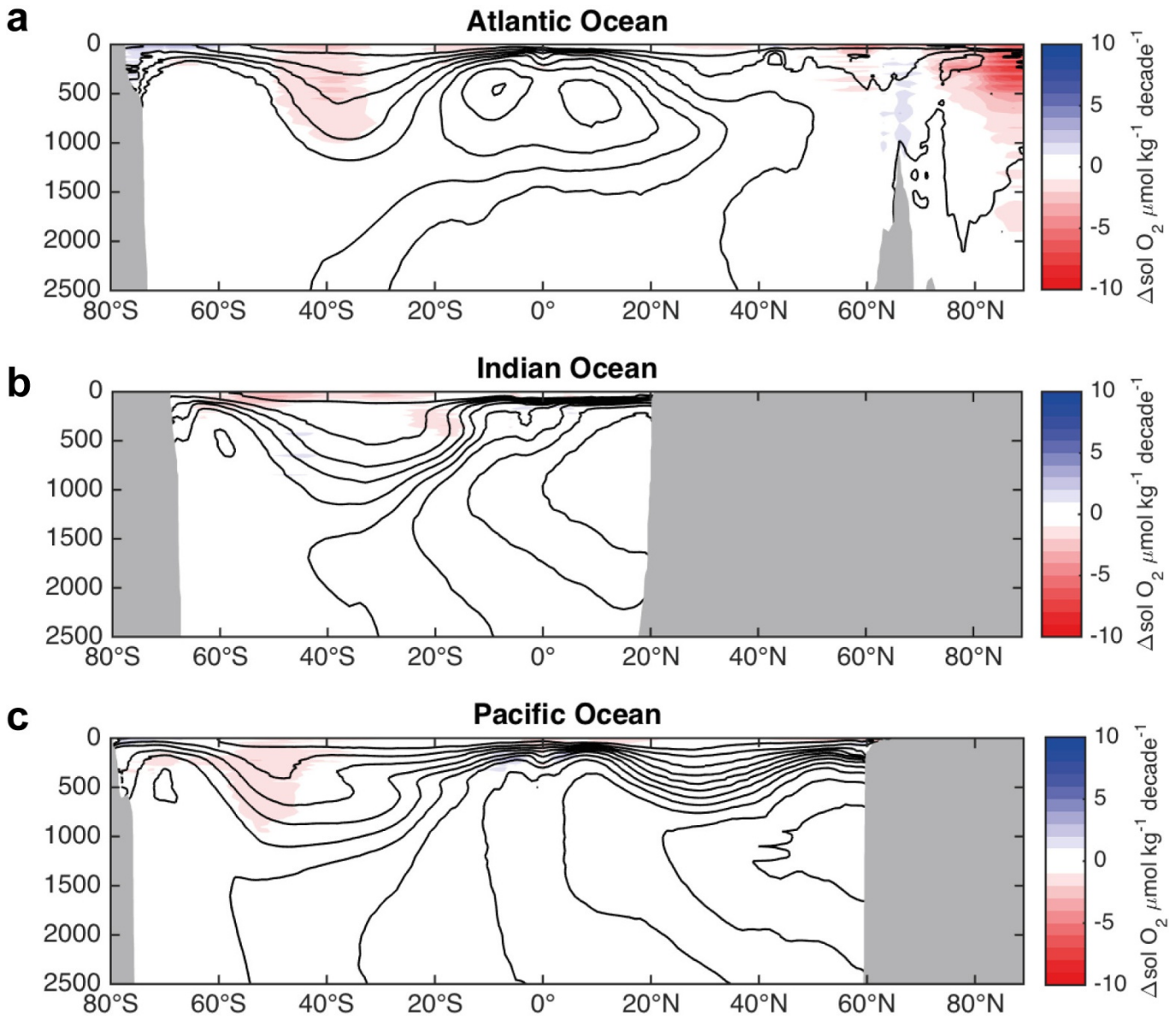

Extended Data Figure 2 | Oxygen solubility changes. a–c, Zonal upper 2,500 m mean oxygen solubility changes in the Atlantic (**a**), Indian (**b**) and Pacific (**c**) oceans. No substantial changes are observed below 1,000 m. Contour lines represent oxygen concentrations at 20 μmol kg^{-1} and every 30 μmol kg^{-1}.

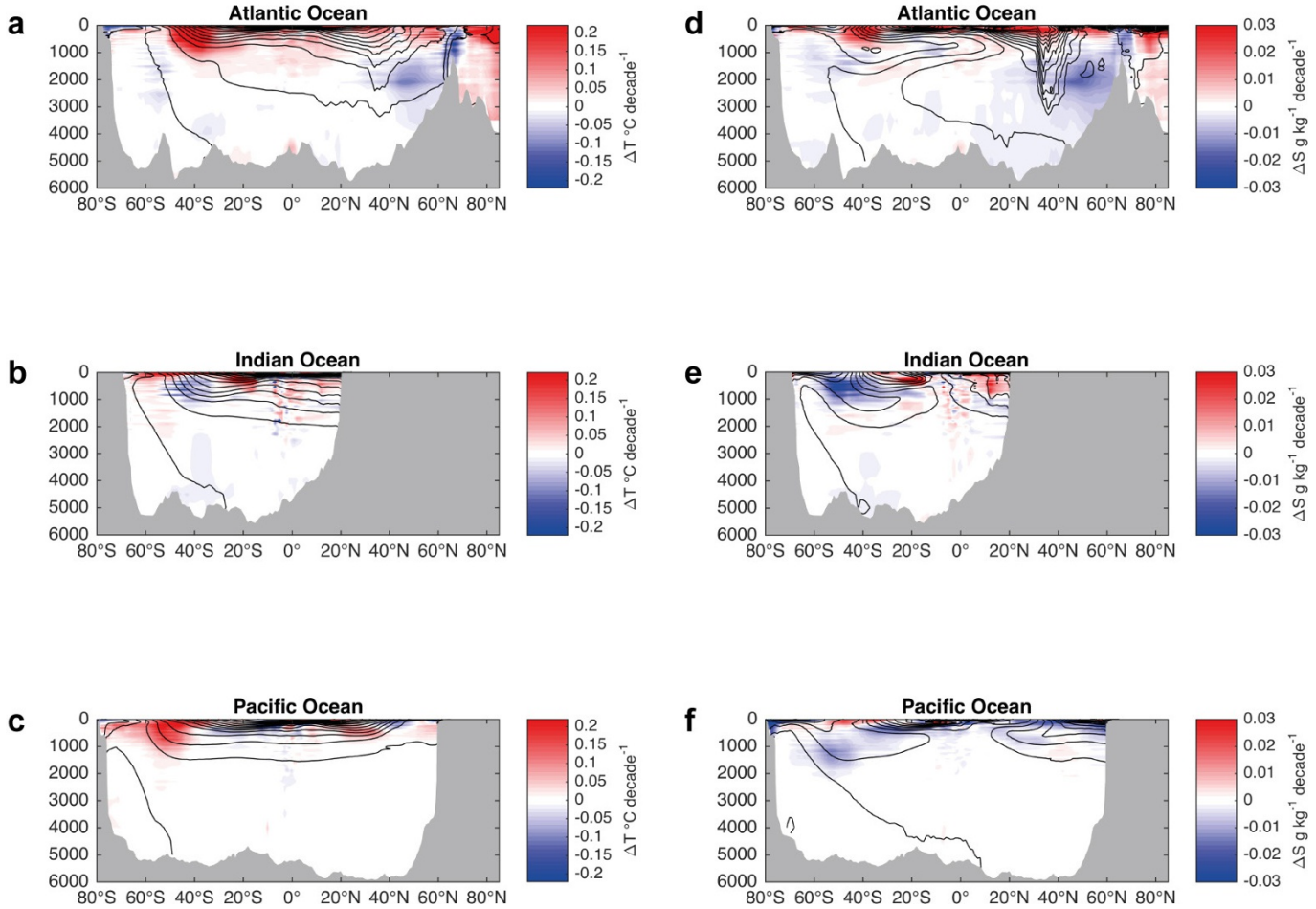

Extended Data Figure 3 | Temperature and salinity changes. a–f, Zonal mean temperature (*T*; **a–c**) and salinity (*S*; **d–f**) changes in the Atlantic (top row), Indian (middle row) and Pacific (bottom row) oceans per decade. Data locations and handling are identical to those used for the oxygen computation and for the results in Extended Data Fig. 1. This is only a small subset of data available for global temperature and salinity trend computations. Contour lines represent the mean fields. Observed trends are similar to trends described in the literature and thus confirm that no artificial trend is created because of sparse or irregular data locations or through the mapping method. Distortions in the North Atlantic around 40° N are due to the Mediterranean Sea, which creates a discontinuity in the zonal means.

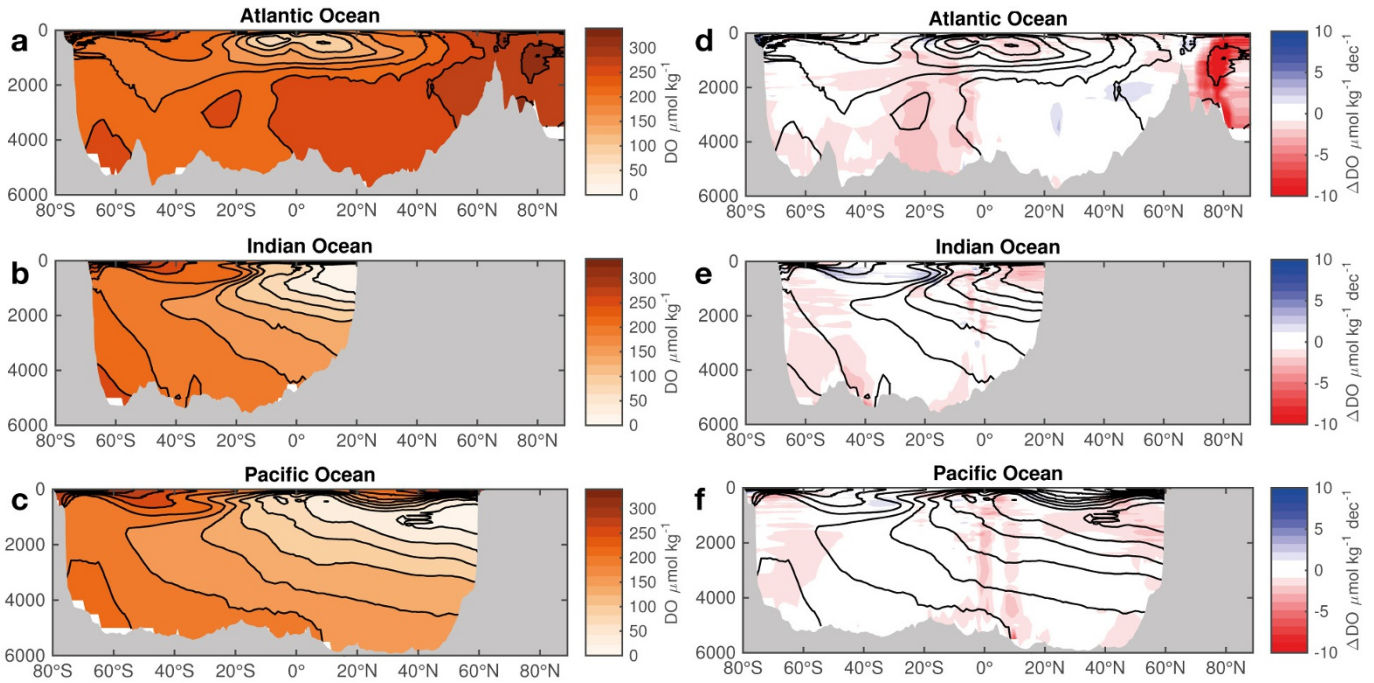

Extended Data Figure 4 | Oxygen concentration and changes. a–f, Zonal mean oxygen concentrations in the Atlantic, Indian and Pacific oceans (**a–c**, respectively), and respective changes in oxygen concentration per decade (**d–f**). Contour lines are at 20 μmol kg^{-1} and every 30 μmol kg^{-1}.

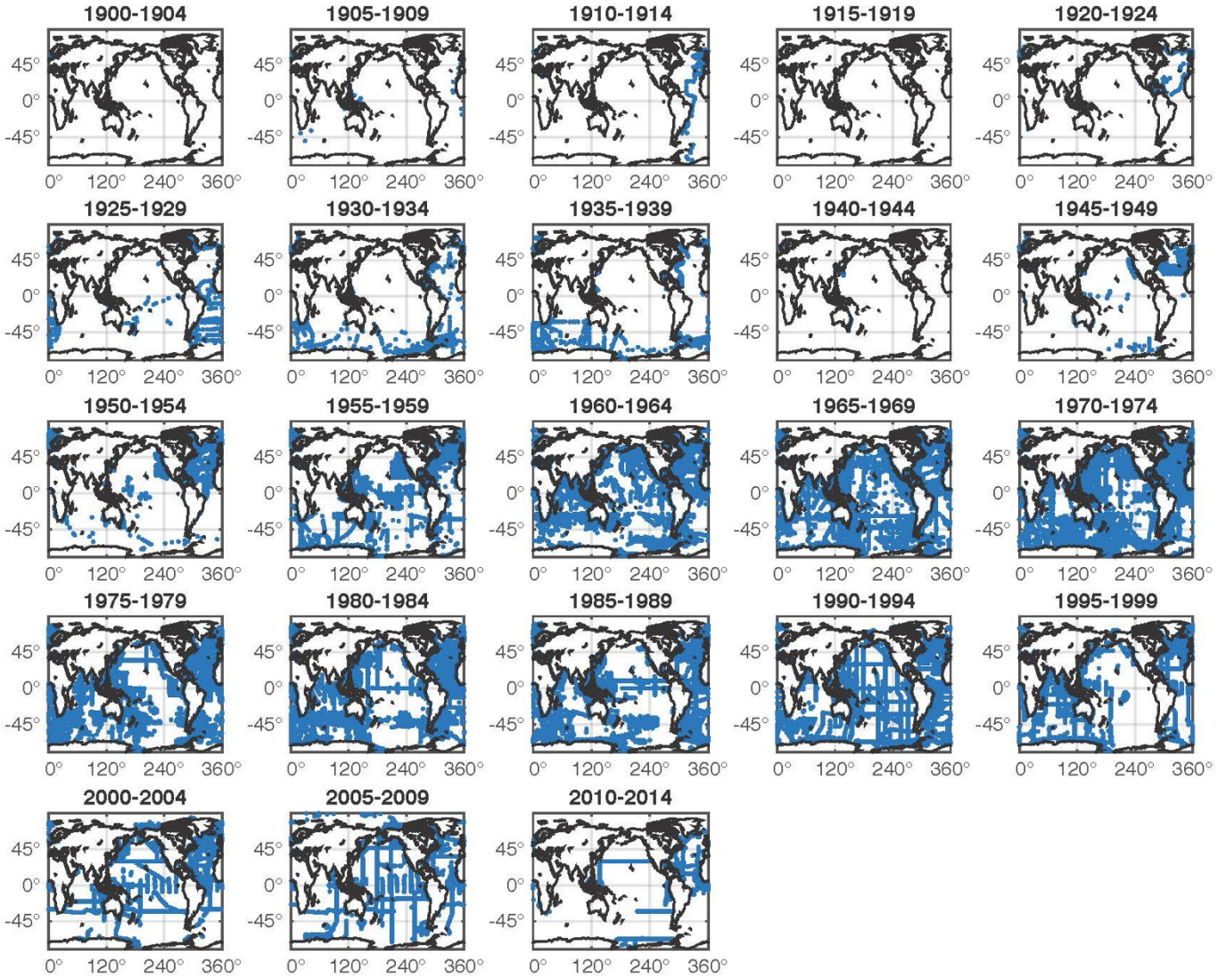

Extended Data Figure 5 | Oxygen profile data coverage since 1900. Blue indicates locations of oxygen profiles over 5-year data intervals, given at the top of each panel.

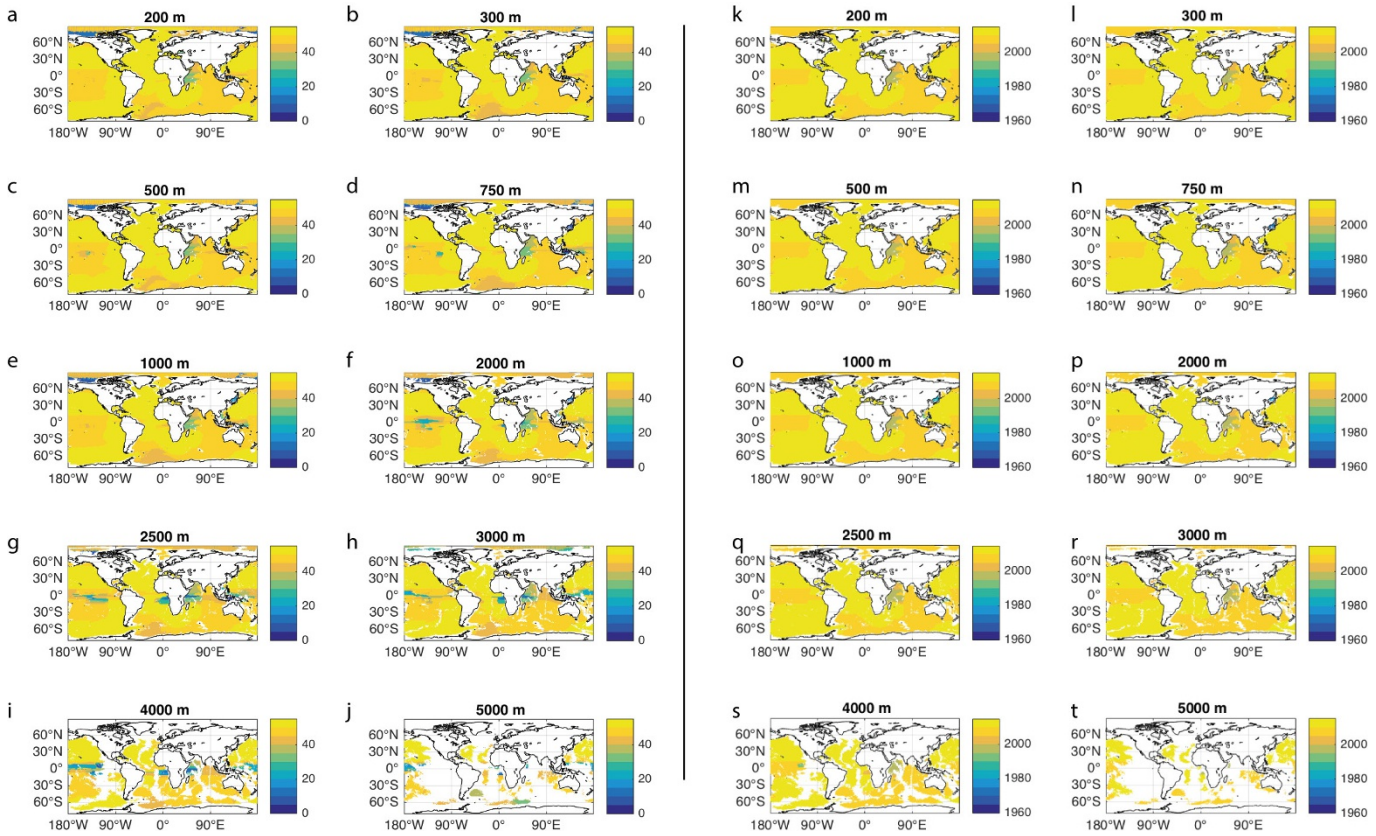

Extended Data Figure 6 | Time span of observations and time of last observation in data sets. a–j, Time span in years is colour coded (key at right of each panel); each panel shows results for the indicated depth layer. **k–t**, Year of last observation of data for each grid point mean state and trend computation is colour coded; each panel shows the results for a particular depth layer.

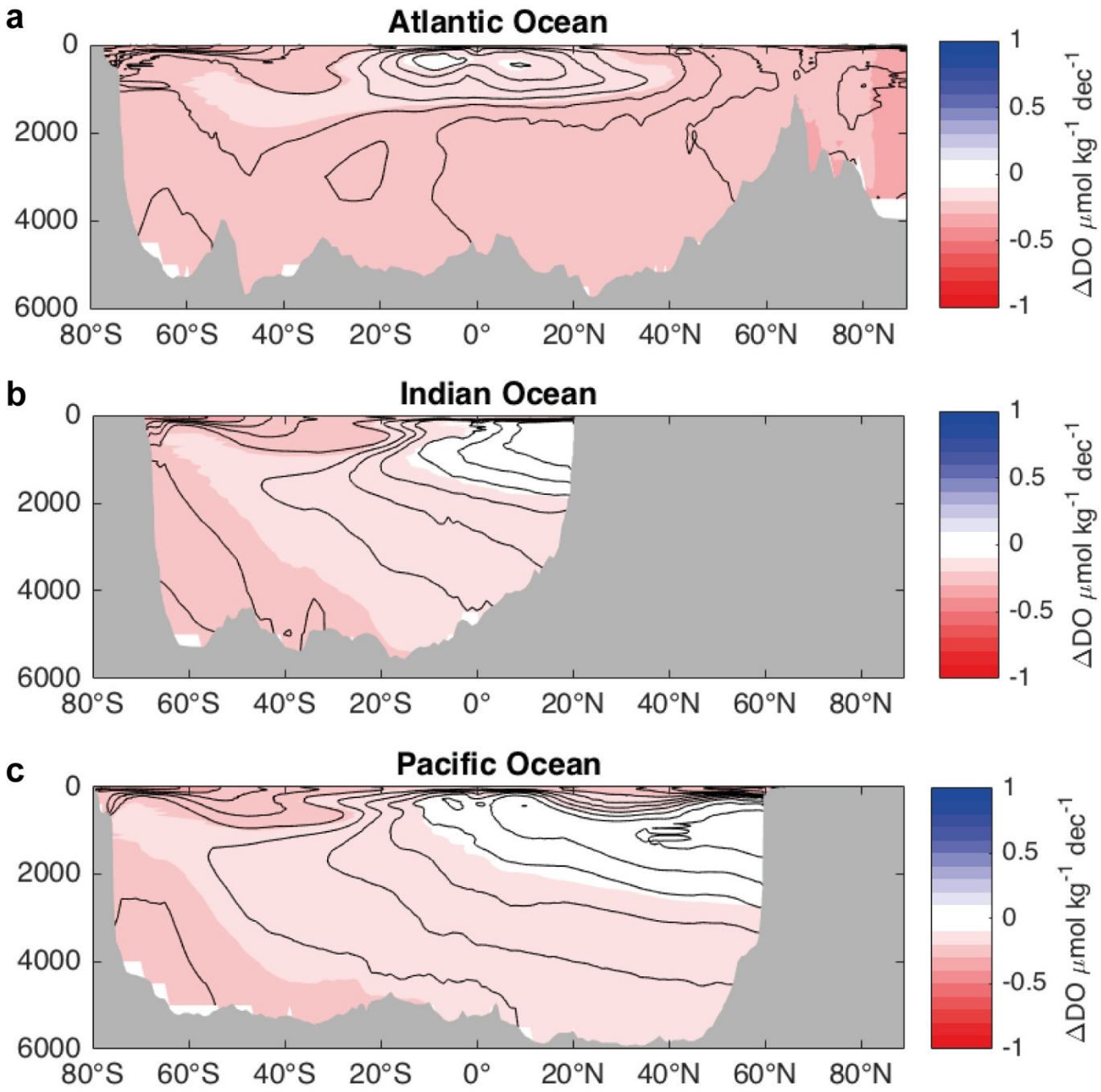

Extended Data Figure 7 | Expected oxygen loss distribution from artificial bias. a–c, Zonal mean changes in dissolved oxygen (colour key at right) of an induced systematic bias of 0.5% for historic measurements (Methods) for Atlantic (**a**), Indian (**b**) and Pacific (**c**) oceans. Note the different order of magnitude of colour scales compared to Extended Data Fig. 4. Solid lines represent the mean oxygen field, as in Extended Data Fig. 4.

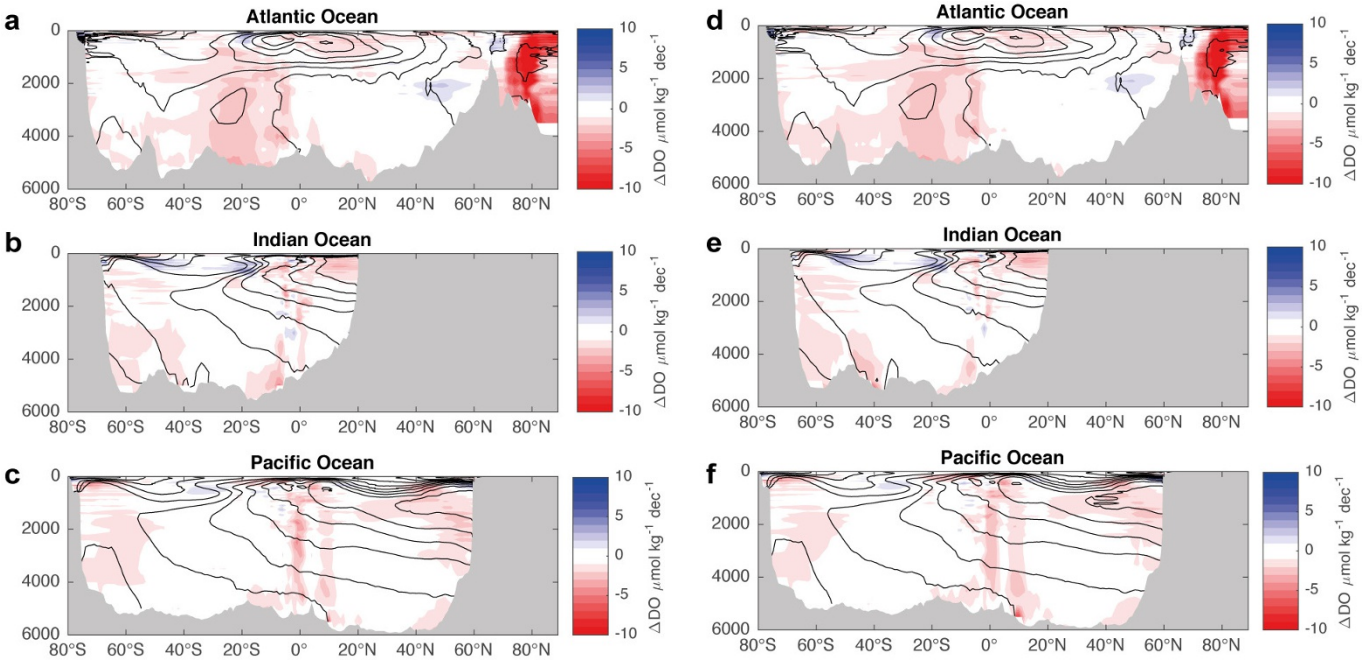

Extended Data Figure 8 | Trend of zonal oxygen loss using reduced data sets. a–f, Change in dissolved oxygen of reduced oxygen data distributions for 20,000 profiles per decade (**a–c**) and 30,000 profiles per decade (**d–f**), validating the robustness of the mapping with 'strongly reduced' and 'reduced' data sets in comparison with the full data set as presented in this Letter (see Methods for details). The global mean trends related to these maps are 946 ± 526 Tmol per decade (**a–c**) and 988 ± 459 Tmol per decade (**d–f**). Solid lines represent the mean oxygen field, as in Extended Data Fig. 4.

Extended Data Table 1 | Volume, oxygen content and change and solubility related changes per basin

Area	Volume (10^6 km^3)	Oxygen Content (Pmol)	Oxygen Change (Tmol/dec^{-1})	Solubility rel. oxy. change (Tmol/dec)	Change in % of global change
Arctic Ocean	15.45	4.73 ± 0.16	-73.1 ± 30.3	-19.2	7.6
0-1200m	7.83	2.42 ± 0.07	-39.9 ± 15.9	-14.7	4.2
1200m-bottom	7.61	2.31 ± 0.09	-33.2 ± 14.5	-4.5	3.5
North Atlantic	111.06	26.86 ± 0.05	-8.5 ± 19.2	-0.4	0.9
0-1200m	34.04	6.90 ± 0.02	-25.6 ± 8.8	-9.8	2.7
1200m-bottom	77.02	19.96 ± 0.03	17.1 ± 10.5	9.3	-1.8
Eq. Atlantic	74.19	15.89 ± 0.04	-72.4 ± 20.2	-11.1	7.5
0-1200m	20.62	2.76 ± 0.02	-22.2 ± 6.7	-7.8	2.3
1200m-bottom	53.58	13.13 ± 0.02	-50.1 ± 13.4	-3.3	5.2
South Atlantic	100.84	22.39 ± 0.05	-119.4 ± 27.4	-30.0	12.4
0-1200m	27.72	5.98 ± 0.02	-13.7 ± 10.8	-26.2	1.4
1200m-bottom	73.12	16.41 ± 0.03	-105.7 ± 16.6	-3.8	11.0
North Pacific	211.67	24.48 ± 0.10	-172.6 ± 40.1	-10.3	18.0
0-1200m	53.68	5.83 ± 0.05	-37.7 ± 18.8	-10.6	3.9
1200m-bottom	158.00	18.65 ± 0.05	-134.9 ± 21.2	0.3	14.1
Eq. Pacific	212.23	25.49 ± 0.40	-210.0 ± 125.2	-3.8	21.9
0-1200m	60.58	5.14 ± 0.09	-67.4 ± 46.0	-1.5	7.0
1200m-bottom	151.65	20.35 ± 0.31	-142.6 ± 79.2	-2.3	14.9
South Pacific	186.29	33.05 ± 0.07	-70.7 ± 36.5	-14.7	7.4
0-1200m	55.75	11.05 ± 0.04	-2.5 ± 18.8	-11.6	0.3
1200m-bottom	130.54	22.00 ± 0.03	-68.2 ± 17.7	-3.1	7.1
Eq. Indian Ocean	85.38	10.74 ± 0.08	-55.0 ± 49.0	-4.9	5.7
0-1200m	26.31	2.09 ± 0.04	-32.0 ± 20.3	-4.3	3.3
1200m-bottom	59.07	8.65 ± 0.04	-23.0 ± 28.7	-0.6	2.4
South Indian Ocean	132.96	26.13 ± 0.06	-26.6 ± 34.3	-1.8	2.8
0-1200m	38.31	8.27 ± 0.03	13.7 ± 14.5	-4.7	-1.4
1200m-bottom	94.64	17.86 ± 0.03	-40.2 ± 19.9	2.8	4.2
Southern Ocean	171.00	37.62 ± 0.09	-152.2 ± 46.9	-34.8	15.8
0-1200m	51.30	11.82 ± 0.05	-30.1 ± 24.5	-25.3	3.1
1200m-bottom	119.70	25.80 ± 0.04	-122.1 ± 22.4	-9.5	12.7
Total:	**1301.07**	**227.38 ± 1.10**	**-960.4 ± 429.1**	**-131.1**	**100.00**
Total 0-1200m:	376.14	62.26 ± 0.43	-257.5 ± 185.1	-116.5	26.8
Total 1200m-bottom:	924.93	165.12 ± 0.67	-702.9 ± 244.0	-14.7	73.2

This is an extended version of Table 1; information has been added about the vertical differences in the basins analysed.

Extended Data Table 2 | Data sources with date of access of data used

Name	Website	Date accessed	Comment
World Ocean Database	http://www.nodc.noaa.gov/OC5/WOD09/pr_wod09.html	05/2013	All CTD and bottle data flagged good or probably good
Hydrobase 3	http://www.whoi.edu/science/PO/hydrobase/	06/2013	All CTD and bottle data used
CLIVAR and Carbon Hydrographic Database	http://cchdo.ucsd.edu/	01/2013	All CTD data available in netCDF format
Southern Ocean Database	http://woceatlas.tamu.edu/Sites/html/atlas/SOA_DATABASE.html	05/2013	All CTD and bottle data used
Pangaea database	http://www.pangaea.de/	05/2013	All Polarstern CTD data publically available

Data can be accessed at http://www.nodc.noaa.gov/OC5/WOD09/pr_wod09.html, http://www.whoi.edu/science/PO/hydrobase/, http://cchdo.ucsd.edu/ and http://www.pangaea.de/; the link to the Southern Ocean Database is no longer active, but the relevant data can be obtained from the corresponding author on reasonable request.